Journal of Materials Chemistry A

Accepted Manuscript

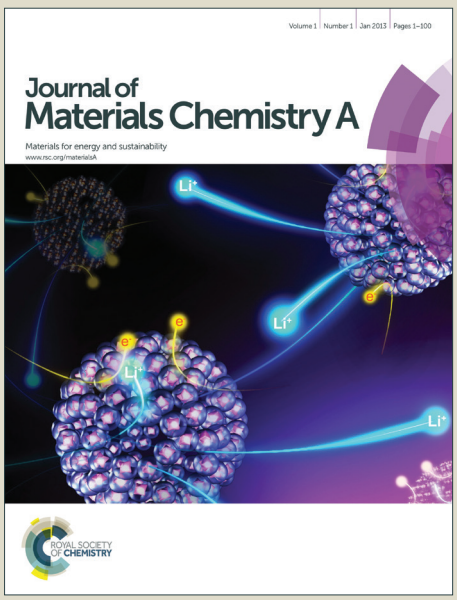

ROYAL SOCIETY OF CHEMISTRY

www.rsc.org/materialsA

Efficient nitrogen-doping and structural control of hierarchical carbons using unconventional precursors in form of deep eutectic solvents

Nieves López-Salas,[a] María C. Gutiérrez,[a] Conchi O. Ania,[b] José Luís G. Fierro,[c] M. Luisa Ferrer,[a] and Francisco del Monte[a, *]

[a] *Instituto de Ciencia de Materiales de Madrid-ICMM, Consejo Superior de Investigaciones Científicas-CSIC. Campus de Cantoblanco, 28049-Madrid (Spain)*

[b] *Instituto Nacional del Carbon-INCAR, Consejo Superior de Investigaciones Científicas-CSIC. C/Francisco Pintado Fe, 26, 33011-Oviedo (Spain)*

[c] *Instituto de Catálisis y Petroleoquímica-ICP, Consejo Superior de Investigaciones Científicas-CSIC. Campus de Cantoblanco, 28049-Madrid (Spain)*

Corresponding author:

Francisco del Monte

Tel.: +34 91 3349033

E-mail: delmonte@icmm.csic.es

Abstract

Since the seminal work by Pekala in 1989, polycondensation of phenol derivatives with formaldehyde and subsequent carbonization has been one of the most used procedures for preparation of porous carbons. Nitrogen-doped carbons have also been obtained through this approach just upon the use of nitrogen-rich precursors. The list of the most commonly used nitrogen-rich-precursors includes melamine, urea, 3-hydroxypyridine, 3-aminophenol or lysine, and despite a few of them can be used in a single fashion, they typically need to be co-condensed with a second precursor. Nitrogen-rich precursors different than these ones have been used rarely because their molecular structure does not favor the nucleophilic substitution though which polycondensation takes place – e.g. p-nitrophenol. This is by no means a trivial issue because, on the one hand, these precursors cannot form a cross-linked network by themselves, and on the other hand, it may be difficult to encompass their different reaction kinetics when combined with more reactive precursors. This is also the situation for other precursors with an amphiphilic molecular structure that could be of interest to control the structure of the resulting porous carbons – e.g. 4-hexylresorcinol. In this work, we have used deep eutectic solvents composed of resorcinol, 4-hexylresorcinol, p-nitrophenol and choline chloride for the preparation of nitrogen-doped carbon monoliths with a hierarchical porous structure. Carbon conversions ranged from 64 to 50% – depending on the carbonization temperature – despite we used three different carbon precursors for co-condensation and two of them were uncommon. The nitrogen content was ca. 3.3 wt%, revealing an excellent nitrogen-doping efficiency for p-nitrophenol when used in form of DES. Finally, the use of 4-hexylresorcinol controlled the formation of a narrow microporosity that, in combination with the nitrogen functionalities, provided a remarkable CO_2-sorption capability to the resulting carbons.

1. Introduction

Nitrogen doped porous carbons (NPC) are attracting considerable interest because of their remarkable performance in number of applications.[1] It is worth noting that nitrogen functionalities provide basic sites and increases the polarity at the porous surface, enhancing the adsorption, separation, catalytic and electrochemical capabilities of NPC as compared to non-doped porous carbons. For instance, it is widely accepted that the use of NPC as electrodes in supercapacitor cells enhances the performance in terms of energy storage because the interaction between electrolyte and nitrogen moieties at the porous surface – by either proton attraction or charge density enhancement of the electrical charge layer – ultimately favors pseudocapacitive contributions.[2, 3, 4] The cathodic oxygen-reduction reaction (ORR) is another field of application for NPCs because they offer an efficient alternative to metal-based electrocatalysts, the replacement of which is critical for the large-scale application of fuel cells.[5, 6, 7, 8] Besides electrochemistry, NPCs have demonstrated an outstanding capability for CO_2 capture[9, 10, 11, 12, 13] considering that presence of nitrogen functionalities promote mechanisms that enhance the CO_2 adsorption capacity and selectivity – including base-acid interaction,[14, 15] quadrupolar interaction,[16] and hydrogen bonds[17] – while preserving the traditional advantages that non-doped porous carbons offer as compared to other sorbents – e.g. cost, availability, large surface area, an easy-to-design pore structure, hydrophobicity and low energy requirements for regeneration, among others.

NPCs have been obtained by different procedures, the carbonization/activation of nitrogen-rich carbon precursors being the most common one. In this case, precursors include polyacrylonitrile,[18] polypyrrol,[19, 20] quinoline pitch,[21] or urea-polymer,[22] among others.[23, 24] More recently, sustainable processes based on direct carbonization of inexpensive and abundant biomass and biomass-derived precursors have also been explored for NPCs preparation.[25] Alternatively, the use of nitrogen-rich ionic liquids (ILs) as precursors has provided NPCs with pore surface areas of ca. 1000 m^2/g and outstanding nitrogen contents of up to 18 at%.[26, 27, 28, 29] Besides direct carbonization, polycondensation of nitrogen-rich precursors with formaldehyde and subsequent

carbonization has also been explored, imitating one of the most common processes used for porous carbons preparation first described by Pekala in 1989 – e.g. polycondensation of resorcinol (Re) with formaldehyde.[30, 31, 32] Melamine is one of the most utilized nitrogen-rich precursor either in a single fashion[2, 3, 33, 34, 35, 36] or co-condensed with a second precursor. In this latter case, phenol derivatives have typically been the precursor of choice[37, 38, 39, 40, 41, 42] but the use of a second nitrogen-rich precursor (e.g. 3-hydroxyaniline) has also been explored.[43] There are other nitrogen-rich precursors like urea, 3-hydroxypyridine, 3-aminophenol or lysine that have been co-condensed with Re offering a suitable alternative to the use of melamine.[14, 34, 38, 44] More recently, polybenzoxazines – first described by Ishida and coworkers[45] – obtained by co-condensation of phenol derivatives and different amines (e.g. bisphenol A and aniline,[46] or Re and 1,6-diaminohexane,[47] among others[48]) with formaldehyde are emerging as a viable alternative for preparation of NPCs. Nonetheless, it is worth noting that neither direct carbonization nor polycondensation procedures are typically capable to provide monolithic NPCs with hierarchical structures comprising pores at different scales – e.g. micro-, meso- and/or macropores – unless structure directing agents – SDA, either soft or hard templates – are used.

Within the context of template-free approaches for carbon monoliths preparation,[49] we have recently described the use of eutectic mixtures containing Re.[50] These eutectic mixtures – first described as deep eutectic solvents (DESs) by Abbott and coworkers[51, 52, 53, 54] – are molecular complexes typically formed between quaternary ammonium salts – e.g. choline chloride (ChCl) or tetraethylammonium chloride (TEA) – and hydrogen-bond donors. The charge delocalization occurring through hydrogen bonding between the halide anion and the hydrogen-donor moiety is responsible for the decrease of the freezing point of the mixture relative to the melting points of the individual components. DESs are considered a sub-group within conventional ILs as they actually share many properties (e.g. non-reactive with water, non-volatile and biodegradable). However, they offer certain advantages as carbon precursors because of their greenness features.[55] Moreover, DES polycondensation with formaldehyde results in the direct – without the

use of any further SDA – formation of monolithic carbons built of highly cross-linked clusters that aggregated and assembled into a stiff and interconnected hierarchical structure.[56, 57, 58] Finally, DES-assisted polycondensations have proved effective in co-condensation processes with some of the carbon precursors mentioned – e.g. 3-hydroxypyridine and 4-hydroxypyridine – for the preparation of hierarchical NPCs in a template-free fashion.[59, 60, 61]

Here in, we explored the capability of DESs for co-condensation processes that might be considered unconventional because of the nature and the number of the carbon precursors that we have used – e.g. 4-hexylresorcinol (4Re) and *p*-nitrophenol (pNP). We also used Re because it helps obtaining good carbon conversions upon the increase of the cross-linking degree. Few reports have described the conventional co-condensation of alkyl derivatives of resorcinol (ARe) and Re, and always using more solvents than just water and low ARe/Re molar ratios.[62] Reports on co-condensation of pNP and Re are also scarce[63] and even more scarce are those ones reporting on co-condensations using three carbon precursors, most likely because of the difficulties to encompass the reaction kinetic of every precursor and, hence, obtain materials containing the moieties introduced upon the use of these precursors – e.g. alkyl and nitrogen groups – homogeneously distributed throughout the whole porous structure. Meanwhile, co-condensation processes using DESs of 3-hydroxypyridine, Re and ChCl,[60] or 4Re, Re and TEA[64] have been capable to overcome these problems because the participation of the carbon precursors in the supramolecular complexes helps encompassing their reaction kinetics. In this work, we have prepared DESs of pNP, 4Re, Re, and ChCl with different molar ratios and we have studied which ones were suitable to obtain NPCs. DESs formation was studied by ^{1}H NMR spectroscopy and differential scanning calorimetry (DSC). The resins resulting from co-condensation were studied by FTIR and solid-state ^{13}C CPMAS NMR spectroscopies. Finally, the NPCs resulting after carbonization were studied by scanning electron microscopy (SEM). The nitrogen content was determined by elemental chemical analysis and X-ray photoelectron spectroscopy (XPS). Nitrogen isotherms at –196 °C were performed to obtain information about the textural properties of the samples. The CO_2

adsorption capability of the resulting carbons was investigated from equilibrium adsorption isotherms at 0 and 25 °C.

2. Experimental Section

2.1. Materials

Resorcinol (Re), *4*-hexylresorcinol (4Re), *p*-nitrophenol (pNP), choline chloride (ChCl) and formaldehyde (37 wt%, aqueous solution) were purchased from Sigma-Aldrich and used as received. Water was distilled and deionized.

2.2. Preparation of DESs

Quaternary DESs $N1_{DES}$, $N2_{DES}$ and $N3_{DES}$ were prepared by physical mixing of Re, 4Re, pNP (as hydrogen donor) and ChCl (as hydrogen acceptor) and subsequent thermal treatment at 90 °C over 60 min. Molar ratio of 1:1:1:1, 1:1:2:1 and 1:1:3:1 were used to obtain $N1_{DES}$, $N2_{DES}$ and $N3_{DES}$, respectively.

2.3. Synthesis of hierarchical carbon monoliths

The polycondensation of the different DESs was accomplished as described elsewhere.[52] Briefly, a formaldehyde aqueous solution (37 wt%) was added to every DES (443 mg of $N1_{DES}$, 582 mg of $N2_{DES}$ and 721 mg of $N3_{DES}$). The molar ratio of formaldehyde versus carbon precursor (resulting from the sum of Re, 4Re and pNP) was always 2. The mixture was homogenized by gently stirring prior addition of the catalyst (0.13 ml of a 140 mg/ml Na_2CO_3 solution). Afterwards, samples were first thermally treated over 6 hours at 60 °C, followed by 7 days at 90 °C. The resins resulting from $N1_{DES}$, $N2_{DES}$ and $N3_{DES}$ were respectively named $N1_{GEL}$, $N2_{GEL}$ and $N3_{GEL}$. Soaking the samples in abundant water three consecutive times washed out any compound eventually entrapped within the porosity of the resulting resins. The washed resins were carbonized at 400, 500, 600, and 800 °C over 4 hours to obtain $N1_{C@X}$, $N2_{C@X}$ and $N3_{C@X}$, where x stands for the temperature used for carbonization.

2.4. Sample characterization

^{1}H NMR spectroscopy was carried out in a Bruker spectrometer DRX-500. DESs were placed in capillary tubes, using deuterated chloroform ($CDCl_3$) or dimethyl sulfoxide

(DMSO) as the external references for spectra recorded at room temperature or 90 °C, respectively. Differential scanning calorimetry (DSC) was performed in a TA Instruments Model DSC Q-100 system, under nitrogen atmosphere. The sample holder – an aluminum pan – was placed in a sealed furnace, stabilized for 30 min at 50 °C, and then cooled to -90 °C before heating at rates of 1 and 10 °C/min. The viscosity of the DESs was measured with a Brookfield Digital Rheometer DV-III fl at 22 °C. Fourier transform infrared (FTIR) spectroscopy was performed in a Bruker Model IFS60v spectrometer. Solid-state ^{13}C CPMAS NMR spectra were obtained using a Bruker Model AV-400-WB spectrometer, by applying a standard cross-polarization pulse sequence. X-Ray Photoelectron spectroscopy (XPS) surface analysis was performed in a VG ESCALAB 200R electron spectrometer equipped with a hemispherical electron analyser and a Mg Kα ($h\upsilon$ = 1253.6 eV, 1 eV = $1.6302 \cdot 10^{-19}$ J) 120 watts X-ray source. Samples were carbon glued on 8 mm diameter stainless steel troughs mounted on a sample rod placed in the pre-treatment chamber and degassed over 30 min prior to being transferred to the analysis chamber. The pressure in the analysis chamber was maintained below 4×10^{-9} mbar during data acquisition. The pass energy of the analyser was set at 50 eV. Charge effects were corrected by fixing the binding energy of the C1s core-level spectrum at 284.9 eV. Data processing was performed with the "*XPS peak*" software, the spectra were decomposed with the least squares fitting routine provided with the software with Gaussian/Lorentzian (90/10) product function and after subtracting a Shirley background. Elemental chemical analysis was performed in an LECO Elemental Analyzer CHNS 932. The technique involved sample combustion at 1000 °C in an oxygen rich environment. CO_2, H_2O and N_2 were carried through the system by He carrier gas and quantitatively measured by means of a non-dispersive IR absorption detection system. N_2 was determined via a thermal conductivity detector.

The morphology of the carbons was studied via scanning electron microscopy (SEM), using a SEM Hitachi S-3000N system. Nitrogen adsorption–desorption isotherms were carried out at –196 °C using an ASAP 2020 from Micromeritics on samples previously degassed under dynamic vacuum (ca. 10^{-5} Torr) at 100 °C for 6 hours. Brunauer-Emmett-

Teller (BET) theory and the Dubinin-Radushkevich method were used to calculate the specific surface areas (S_{BET}) and micropore volumes, respectively. CO_2 adsorption–desorption isotherms were performed at 0 and 25 °C in a Micromeritics Tristar 3020 instrument in the pressure range of 0.1-900 mbar.

3. Results and discussion

$N1_{DES}$, $N2_{DES}$ and $N3_{DES}$ were prepared by physical mixing of Re, 4Re, pNP – as hydrogen donors – and ChCl – as hydrogen acceptor – in different molar ratios (e.g. 1:1:1:1, 1:1:2:1 and 1:1:3:1, respectively). Subsequently, the solid mixture was molten upon thermal treatment at 90 °C over 60 min. For every of the used molar ratios, the molten mixtures remained in the liquid phase when returned to room temperature. $N1_{DES}$, $N2_{DES}$ and $N3_{DES}$ were investigated by differential scanning calorimetry (DSC). Neither melting temperature (T_m) nor crystallization temperature (T_c) was displayed in the DSC trace of any of the studied DESs (Fig. 1) which is a common feature observed for non-easily crystallizable ILs and DESs. $N1_{DES}$, $N2_{DES}$ and $N3_{DES}$ were all viscous liquids, the viscosities of which at room temperature (e.g. 2636, 2015 and 1548 cP, respectively) decreased along with the pNP content in the mixture in agreement with the evolution of their glass transition temperatures (see T_g in Fig. 1).[65] The up-field chemical shift of the signals that every of the DES-forming-components experienced at the ^{1}H NMR spectra – as compared to those of the individual components – confirmed not only the presence of H-bond complexes in the DESs but also their quaternary character (Fig. 2 and Table 1). Otherwise – i.e. in case one or two of the precursors are just dissolved in the respective ternary or binary DES, the chemical shifts of the dissolved precursors would be closer to those of the individual components.

Moreover and to fully clarify this issue, we prepared three different DESs using every single precursor and ChCl. Thus, the first DES was composed of Re:ChCl, the second one of 4Re:ChCl, and the third one of pNP:ChCl, with a 3:1 molar ratio in every case. The chemical shifts at the ^{1}H NMR spectra revealed the typical behavior observed for DESs, this is, they were all up-field shifted as compared to those of the individual components (Fig. S1 and

S2, and Table S1, in ESI). It is worth noting that spectra were recorded at 90 °C – and hence, using DMSO rather than $CDCl_3$ as the external reference – because the melting point of some of these binary DESs was above room temperature. Interestingly, the mixture of them would provide a quaternary mixture with the molar stoichiometry of $N1_{DES}$ (1:1:1:1).

The polycondensation of $N1_{DES}$, $N2_{DES}$ and $N3_{DES}$ was carried out in basic conditions (Na_2CO_3) by the addition of a formaldehyde solution (37 wt%). This addition resulted in a DES dilution to about 54, 52, and 51 wt%, respectively. One may wonder whether this DES dilution should still be considered as a DES or just as a simple aqueous solution of the individual components that were forming the DES. We addressed this question by recording the ^{1}H NMR spectrum of the aqueous dilutions of DES.[66, 67, 68] We found that the chemical shifts of the diluted DESs were in between those of neat DES and those of the individual components that formed the DES – or even more similar to these latter ones (Fig. S3 and Table S2, in ESI). Interestingly, we have previously reported how this synthetic process benefits from the partial rupture of the ion-hydrogen-bond-donor supramolecular complexes that characterize DESs because (a) part of the DES-components will be readily available for polycondensation, and (b) the non-available ones will contribute to the phase separation that determines the ultimate morphology of the resulting materials.[46] Whether this a-plus-b-based mechanism also applies to the polycondensation of Re, 4Re and pNP was studied in detail by FTIR and solid-state ^{13}C CPMAS NMR spectroscopies. Nonetheless, the former was anticipated by the formation of monolithic resins (Fig. 3) and the latter by the presence of DES components that not participated in the polycondensation. These DES components were obtained upon washing the resulting gels with abundant water (three consecutive times with 35 mL each). As described in previous reports, ChCl segregation during polycondensation allowed its fully recovering. In this case, part of pNP was also recovered upon washing, the molar ratio of which was always the same – e.g. 0.15 referred to ChCl – for $N1_{GEL}$, $N2_{GEL}$ and $N3_{GEL}$ (Fig. S4 in ESI). We further studied the nature of the pNP:ChCl mixture with a molar ratio of 0.15:1. They could not be classified as a DES because the melting point was above 100 °C. Interestingly, the chemical shifts of the

signals in the ^{1}H NMR spectrum of the pNP:ChCl mixture diluted in D_2O were upfield shifted as compared to the individual components (Fig. S5 and Table S3 in ESI). This was actually the case in both neat and diluted DESs (compare with data in Tables 1 and S2 in ESI) so we speculated that the pNP:ChCl mixture is also forming a H-bond complex. XRD revealed the crystalline nature of this H-bond complex, with a structure that is different than any of the forming compounds (Fig. S6 in ESI).

Co-condensation between Re, 4Re and pNP was further assessed in the washed resins by FTIR and solid-state ^{13}C CPMAS NMR spectroscopies. As mentioned in the introduction, the use of 4Re and/or pNP as precursors has been rarely explored because polycondensation is much less favored than for Re. For instance and with regard to 4Re, the hexyl group blocks one of the aromatic-ring positions that is susceptible of nucleophilic substitution. Meanwhile, the nitro substituent in pNP induces deactivation in the aromatic ring. Thus, both precursors would tend to form linear rather than cross-linked polymers unless one uses them as additional precursors besides Re, as in our case. The observation of bands at the FTIR spectrum assigned to methylene (C–H stretching and bending modes at ca. 2945 and 1473 cm^{-1}, respectively) and to methylene oxide groups (C–O benzyl ether groups at about 1091 and 1220 cm^{-1}) are typically indicative of a significant number of linkages between Re rings (Fig. 4).[69] However, the correlation between methylene groups with the number of bridges established upon polycondensation must be taken with caution in this case. It is worth remembering that methylene groups of 4Re will also contribute to the overall intensity of these bands. Actually, we obtained more intense signals in this case than in previous ones dealing with self-condensation of Re[52] whereas the opposite should be expected considering the above-explained reactivity of Re and 4Re. This feature was further corroborated by the intensity of the bands attributed to methylene stretching and bending vibrations – at 2920 and 2850 cm^{-1}. Meanwhile, the co-condensation of pNP was confirmed by the presence of the bands at ca. 1337 and 1487 cm^{-1} that correspond to the symmetric and asymmetric stretching vibration of the nitro group bonded to the aromatic carbon.[70, 71, 72]

Solid-state ^{13}C CPMAS NMR spectroscopy provided further insights with regard to the polycondensation issue (Fig. 5). As FTIR, NMR revealed the presence of methylene ether (e.g. CH_2–O–CH_2 at ca. 53 ppm) and methylene (e.g. CH_2 at 31 and 23 ppm) groups adjacent to the aromatic ring,[73, 74] the peak intensity of these latter ones being higher than in single Re-based resins due to the use of 4Re as precursor.[59] The signals at about 116 and 131 ppm were more useful in terms of polycondensation. The former corresponded to aromatic carbons bearing CH_2 groups in all ortho positions relative to the two phenolic OHs and the latter to non-substituted aromatic carbons in meta positions so that their relative intensity allows quantifying the nucleophilic positions that participated in the polycondensation – i.e. in comparison with the polycondensations that use Re as a single precursor. The incorporation of pNP and 4Re into the co-condensed network was confirmed, in the former case, by the presence of peaks at ca. 164 and 140 ppm – assigned to the aromatic carbons bearing the hydroxyl and the nitro groups, respectively – and at 126 ppm – assigned to the aromatic carbons in meta positions to the carbon bearing the hydroxyl group – while, in the latter one, by the presence of a peak at 122 ppm – assigned to the aromatic carbons bearing the hexyl chain.[75] The signal at 14 ppm further corroborated the presence of methylene groups coming from the hexyl moiety pending from the aromatic ring of 4Re.

The good extension in which pNP, 4Re and Re co-condensed was corroborated by the carbon conversions (e.g. 50–64%, see Table 2) that were obtained after carbonization of the washed gels at different temperatures – i.e. from 400 to 800 °C in a N_2 atmosphere. It is worth noting that, despite conversions above 70% – at 800 °C – have been previously reported for DES-assisted co-condensations between Re and either 3-hydroxypyridine or 4Re, conventional co-condensations have rarely reached conversions above 50% even though more-favorable-for-condensation precursors are typically used (e.g. Re with 3-hydroxypyridine, Re with melamine, or Re with 3-aminophenol, among others).[34, 38] Moreover, we should also take into account that we were using three – rather than just two – precursors, only Re was particularly favorable in condensation terms, and the molar ratio of the secondary precursors versus Re was higher than in conventional co-

condensations (see Table 2). SEM micrographs corroborated the formation of hierarchical porous structures that are typically obtained via DES-assisted polycondensations (Fig. 6 and 7, and Fig. S7-S9 in ESI). We have previously described how DESs are responsible of the formation of morphologies in form of a bicontinuous porous network composed of highly crosslinked clusters that aggregated and assembled into a stiff, interconnected structure. In this particular case, co-condensation of Re, 4Re and pNP resulted in the formation of a polymer-rich phase that was accompanied by the segregation of the noncondensed matter (e.g. ChCl) creating first a polymer-poor phase that, ultimately, becomes a polymer-depleted phase. This phase-separation process ended with the formation of an aggregates-of-particles-like morphology. It is worth noting that the transient structure that results from phase separation has been correlated to the time relation between the onset of phase separation and gel formation – e.g. interconnected structures if the onset of both processes coincide or particle aggregates if phase segregation occurs earlier than gel formation.[76] This latter case where the polymer-rich domains break-up and become spherical during the coarsening process of the spinodal decomposition in order to decrease the interfacial energy before the structure freezing[77] corresponds well with the morphology of our samples.

Besides morphology control, the use of DES-assisted co-condensations aimed introducing certain functionalities in the resulting carbon. For instance, the DES-assisted co-condensation of Re and 3-hydroxypyridine produced nitrogen-doped carbons while the DES-assisted co-condensation of Re and 4Re produced carbons with a narrow microporosity. In this case, we produced carbons that simultaneously exhibited nitrogen functionalities and narrow microporosity because of the concurrent use of pNP and 4Re as precursors. Thus, the use of pNP was responsible of the production of carbons with a certain nitrogen content – from 4.9 to 3.3 wt% depending on the starting DES composition and carbonization temperature, see Fig. 8. The nitrogen content of the carbons obtained at 800 °C was in range to those obtained in most of conventional co-condensations – e.g. 3.7 wt% using phenol and melamine,[33] 3.5 wt% using Re and melamine,[35] or 4.4 wt% using Re and 3-hydroxypyridine (Table 2).[38] Higher nitrogen contents – up to 13.3 wt% – have

been obtained in some particular conventional co-condensations where the nitrogen content of the precursors was extremely high – e.g. phenol and melamine with molar ratios ranging from 1:1 to 1.2,[32] or melamine and 3-hydroxypyridine with a 1:0.6 molar ratio, among others (Table 2).[38] Nonetheless, the nitrogen-doping efficiency – estimated as the ratio between the N/C atomic ratio at the precursors versus the N/C atomic ratio at the resulting carbon – of conventional syntheses was in every case far below that of DES-assisted ones. Thus, the best nitrogen-doping efficiency found in the former cases was 58% – for the recently-described polybenzoxazines prepared from bisphenol A and aniline[42] – whereas in the latter ones, $N1_{C@800}$ reached a remarkable nitrogen-doping efficiency of 78% (see Table 2).

We also studied the nitrogen functionalities of $N3_{C@500}$ and $N3_{C@800}$ by XPS. Up to five types of nitrogen (pyridinic-N at 398.7 ± 0.3 eV, pyrrolic-N or pyridone-N at 400.3 ± 0.3 eV, quaternary-N at 401.4 ± 0.5 eV and oxidized-N at 402–405 eV) are typically distinguished in nitrogen-doped carbons.[78, 79] In our case, pyrrolic-N or pyridone-N, and pyridinic-N were the main nitrogen types when the thermal treatment was 500 °C, while quaternary-N (graphitic)[38] and oxidized-N could be observed but in a minor percentage. This distribution was similar to that found for NPCs obtained at 600 °C when the nytrogen-rich precursor forming the DES was 3-hydroxypyridine rather than pNP. Upon further thermal treatment at 800 °C, the contribution of pyridinic-N and quaternary-N was maintained whereas there was a significant enhancement of the contribution of pyrrolic-N or pyridone-N mostly at the expenses of oxidized-N (Fig. 9 and Table S4). In this case, the XPS xpectrum of $N3_{C@800}$ revealed that the contributions of quaternary-N and oxidized-N evolved with the temperature used for carbonization differently – the former experienced a significant increase while the latter was completely depleted – than those found for carbons obtained at 800 °C from DESs containing 3-hydroxypyridine.[59]

Meanwhile, the use of 4Re was responsible of the narrow microporosity of the resulting carbons. This feature was first assessed by nitrogen adsorption–desorption isotherms at –196 °C. The N_2 uptake was negligible for every of the synthesized carbons (Table 3) but the CO_2 adsorption isotherms at 0 °C revealed a remarkable CO_2 adsorption

capacity with uptakes of up to 3.8 mmol/g at 760 mbar in range to or even better than some of the most remarkable sorption capacities found for NPCs and even KOH-activated NPCs (Fig. 10, Table 4). The application of the Dubinin-Radushkevich and Stoeckli–Ballerini equations to the CO_2 adsorption isotherms allowed the calculation of the micropore volume (W_o) and the average micropore size (L), respectively (Table 3). The latter provided an average micropore diameter for every sample of ca. 0.56 nm. The restricted diffusion of N_2 at –196 °C through micropores of such small dimensions explains the negligible N_2 uptake described above.

4. Conclusion

We have described the synthesis of three different DES based on Re, 4Re and pNP – as hydrogen donors – and ChCl – as hydrogen acceptor upon the addition of different amounts of pNP. The resulting DESs were co-condensed with formaldehyde for the production – upon carbonization – of nitrogen-doped carbon monoliths with a hierarchical porous (bimodal, with macropores and micropores) structure. The resulting carbons exhibited an excellent CO_2 adsorption capacity – with uptakes of up to 3.8 mmol/g at 900 mbar – thanks to the concurrent presence of nitrogen functionalities and narrow microporosity. It is worth noting that, in this work, nitrogen was introduced – up to 3.7 wt% at 800 °C – upon the use of a precursor like pNP that is not particularly favorable for condensation and, despite of it, the nitrogen-doping efficiency exceeded that of conventional syntheses carried out with more favorable carbon precursors. These results corroborated the capability of DES-assisted co-condensation for preparation of nitrogen-doped carbons. Finally, the DESs capability to encompass the kinetic reaction of different precursors was further emphasized by their capability to also co-condense 4Re, the use of which as a third precursor provided the above-mentioned narrow microporosity that characterized the resulting carbons.

Acknowledgements

This work was supported by MINECO (MAT2012-34811 and MAT2011-25329). NLS and JP acknowledge MINECO for respective FPI contracts.

References

1 P. Ayala, R. Arenal, M. Rümmeli, A. Rubio, and T. Pichler, "The doping of carbon nanotubes with nitrogen and their potential applications" *Carbon* **2010**, *48*, 575-586

2 D. Hulicova, J. Yamashita, Y. Soneda, H. Hatori, and M. Kodama, "Supercapacitors Prepared from Melamine-Based Carbon" *Chem. Mater.* **2005**, *17*, 1241–1247.

3 D. Hulicova-Jurcakova, M. Kodama, S. Soshi, H. Hatori, Z. H. Zhu, and G. Q. Lu, "Nitrogen-Enriched Nonporous Carbon Electrodes with Extraordinary Supercapacitance" *Adv. Funct. Mater.* **2009**, *19*, 1800–1809.

4 M. Hughes, M. S. P. Shaffer, A. C. Renouf, C. Singh, G. Z. Chen, D. J. Fray, and A. H. Windle, "Electrochemical Capacitance of Nanocomposite Films Formed by Coating Aligned Arrays of Carbon Nanotubes with Polypyrrole" *Adv. Mater.* **2002**, *14*, 382–385.

5 K. Gong, F. Du, Z. Xia, M. Durstock, and L. Dai, "Nitrogen-Doped Carbon Nanotube Arrays with High Electrocatalytic Activity for Oxygen Reduction" *Science* **2009**, *323*, 760–764

6 L. Qu, Y. Liu, J.-B. Baek, and L. Dai, "Nitrogen-Doped Graphene as Efficient Metal-Free Electrocatalyst for Oxygen Reduction in Fuel Cells" *ACS Nano* **2010**, *4*, 1321–1326

7 J. D. Wiggins-Camacho, and K. J. Stevenson, "Mechanistic Discussion of the Oxygen Reduction Reaction at Nitrogen-Doped Carbon Nanotubes" *J. Phys. Chem. C* **2011**, *115*, 20002–20010

8 R. Liu, D. Wu, X. Feng, and K. Müllen, "Nitrogen-Doped Ordered Mesoporous Graphitic Arrays with High Electrocatalytic Activity for Oxygen Reduction" *Angew. Chem.* **2010**, *49*, 2565–2569

9 Y. Zhao, L. Zhao, K. X. Yao, Y. Yang, Q. Zhang, and Y. Han, "Novel porous carbon materials with ultrahigh nitrogen contents for selective CO_2 capture" *J. Mater. Chem.* **2012**, *22*, 19726–19731

10 Y. Zhao, X. Liu, K. X. Yao, L. Zhao, and Y. Han, "Superior Capture of CO2 Achieved by Introducing Extra-framework Cations into N□doped Microporous Carbon" *Chem. Mater.* **2012**, *24*, 4725–4734

11 J. Wei, D. Zhou, Z. Sun, Y. Deng, Y. Xia, and D. Zhao, "A Controllable Synthesis of Rich Nitrogen-Doped Ordered Mesoporous Carbon for CO 2 Capture and Supercapacitors" *Adv. Funct. Mater.* **2013**, *23*, 2322–2328

12 X. Fan, L. Zhang, G. Zhang, Z. Shu, and J. Shi, "Chitosan derived nitrogen-doped microporous carbons for high performance CO_2 capture" *Carbon* **2013**, *61*, 423–430

13 X. Ma, M. Cao, and C. Hu, "Bifunctional HNO3 catalytic synthesis of N-doped porous carbons for CO2 capture" *J. Mater. Chem. A* **2013**, *1*, 913–918

[14] G. P. Hao, W. C. Li, D. Qian, and A. H. Lu, "Rapid Synthesis of Nitrogen-Doped Porous Carbon Monolith for CO_2 Capture**"** *Adv. Mater.* **2010**, *22*, 853–857.

[15] L. Wang and R. T. Yang, "Significantly Increased CO_2 Adsorption Performance of Nanostructured Templated Carbon by Tuning Surface Area and Nitrogen Doping" *J. Phys. Chem. C* **2012**, *116*, 1099–1106

[16] R. Vaidhyanathan, S. S. Iremonger, G. K. Shimizu, P. G. Boyd, S. Alavi, and T. K. Woo, "Direct Observation and Quantification of CO_2 Binding Within an Amine-Functionalized Nanoporous Solid" *Science* **2010**, *330*, 650–653

[17] W. Xing, C. Liu, Z. Zhou, L. Zhang, J. Zhou, S. Zhuo, Z. Yan, H. Gao, G. Wang, and S. Z. Qiao, "Superior CO_2 uptake of N-doped activated carbon through hydrogen-bonding interaction" *Energy Environ. Sci.* **2012**, *5*, 7323–7327.

[18] W. Shen, S. Zhang, Y. He, J. Li, and W. Fan, "Hierarchical porous polyacrylonitrile-based activated carbon fibers for CO2 capture" *J. Mater. Chem.* **2011**, *21*, 14036-14040

[19] M. Sevilla, P. Valle-Vigón, and A. B. Fuertes, "N-Doped Polypyrrole-Based Porous Carbons for CO_2 Capture" *Adv. Funct. Mater.* **2011**, *21*, 2781–2787

[20] L. Qie, W.-M. Chen, Z.-H. Wang, Q.-G. Shao, X. Li, L.-X. Yuan, X.-L. Hu, W.-X. Zhang, and Y.-H. Huang "Nitrogen-Doped Porous Carbon Nanofiber Webs as Anodes for Lithium Ion Batteries with a Superhigh Capacity and Rate Capability" *Adv. Mater.* **2012**, *24*, 2047-2050

[21] E. Raymundo-Piñero, D. Cazorla-Amorós, A. Linares-Solano, J. Find, U. Wild, and R. Schlögl, "Structural characterization of N-containing activated carbon fibers prepared from a low softening point petroleum pitch and a melamine resin" *Carbon* **2002**, *40*, 597-608.

[22] W. Shen, T. Hu, P. Wang, H. Sun, and W. Fan, "Hollow porous carbon fiber from cotton with nitrogen doping" *ChemSusChem* **2014**, *79*, 284-289

[23] F. Stoeckli, T. A. Centeno, A. B. Fuertes, and J. Muñiz, "Porous structure of polyarylamide-based activated carbon fibres" *Carbon* **1996**, *34*, 1201-1206

[24] D. Hulicova-Jurcakova, M. Seredych, G. Q. Lu, and T. J. Bandosz, "Combined effect of nitrogen- and oxygen-containing functional groups of microporous activated carbon on its electrochemical performance in supercapacitors" *Adv. Funct. Mater.* **2009**, *19*, 438-447

[25] R. J. White, M. Antonietti, and M. M. Titirici, "Naturally inspired nitrogen doped porous carbon" *J. Mater. Chem.* **2009**, *19*, 8645-8650

[26] J. P. Paraknowitsch, J. Zhang, D. Su, A. Thomas, and M. Antonietti, "Ionic Liquids as Precursors for Nitrogen-Doped Graphitic Carbon" *Adv. Mater.* **2010**, *22*, 87–92.

[27] J. S. Lee, X. Wang, H. Luo, G. A. Baker, and S. Dai, "Facile Ionothermal Synthesis of Microporous and Mesoporous Carbons from Task Specific Ionic Liquids" *J. Am. Chem. Soc.* **2009**, *131*, 4596–4597

[28] J. P. Paraknowitsch, A. Thomas, and M. Antonietti, "A detailed view on the polycondensation of ionic liquid monomers towards nitrogen doped carbon materials" *J. Mater. Chem.* **2010**, *20*, 6746–6758.

[29] J. S. Lee, X. Wang, H. Luo, and S. Dai, "Fluidic Carbon Precursors for Formation of Functional Carbon under Ambient Pressure Based on Ionic Liquids" *Adv. Mater.* **2010**, *22*, 1004–1007.

[30] R. W. Pekala, "Organic aerogels from the polycondensation of resorcinol with formaldehyde" *J. Mater. Sci.* **1989**, *24*, 3221

[31] A. Taguchi, J.-H. Smatt, and M. Lindén, "Carbon Monoliths Possessing a Hierarchical, Fully Interconnected Porosity." *Adv. Mater.* **2003**, *15*, 1209.

[32] S. A. Al-Muhtaseb, and J. A. Ritter, "Preparation and Properties of Resorcinol–Formaldehyde Organic and Carbon Gels" *Adv. Mater.* **2003**, *15*, 101.

[33] Y.-R. Dong, N. Nishiyama, M. Kodama, Y. Egashira, and K. Ueyama, "Nitrogen-containing microporous carbons prepared from anionic surfactant-melamine/formaldehyde composites" *Carbon* **2009**, *47*, 2112−2142.

[34] D. F. Schmidt, C. du Fresne von Hohenesche, A. Weiss, and V. Schädler "Colloidal Gelation as a General Approach to the Production of Porous Materials" *Chem. Mater.* **2008**, *20*, 2851–2853.

[35] C. Pevida, T. C. Drage, and C. E. Snape, "Silica-templated melamine-formaldehyde resin derived adsorbents for CO_2 capture" *Carbon* **2008**, *46*, 1464-1474.

[36] E. Masika and R. Mokaya, "High surface area metal salt templated carbon aerogels via a simple subcritical drying route: preparation and CO_2 uptake properties" *RSC Advances* **2013**, *3*, 17677-17681.

[37] H. Chen, F. Sun, J. Wang, W. Li, W. Qiao, L. Ling, and D. Long, "Nitrogen Doping Effects on the Physical and Chemical Properties of Mesoporous Carbons" *J. Phys. Chem.* **2013**, *117*, 8318−8328.

[38] D. Long, J. Zhang, J. Yang, Z. Hu, G. Cheng, X. Liu, R. Zhang, L. Zhan, W. Qiao, and L. Ling, "Chemical state of nitrogen in carbon aerogels issued from phenol–melamine–formaldehyde gels" *Carbon* **2008**, *46*, 1253−1269.

[39] P. Veselá, V. Slová, "Pyrolysis of N-doped organic aerogels with relation to sorption properties" *J. Therm. Anal. Calorim.* **2012**, *108*, 470-475.

[40] H. F. Gorgulho, F. Goncalves, M. F. R. Pereira, and J. L. Figueiredo, "Synthesis and characterization of nitrogen-doped carbon xerogels" *Carbon* **2009**, *47*, 2032-2039.

[41] J. Yu, M. Guo, F. Muhammad, A. Wang, G. Yu, H. Ma, and G. Zhu, "Simple fabrication of an ordered nitrogen-doped mesoporous carbon with resorcinol–melamine–formaldehyde resin" *Micro. Meso Mater* **2014**, *190*, 117−127.

[42] R. Zhang, Y. Lu, L. Zhan, X. Liang, G. Wu, and L. Ling, "Monolithic carbon aerogels from sol–gel polymerization of phenolic resoles and methylolated melamine" *Carbon* **2003**, *411*, 1645−1687.

[43] M. Pérez-Cadenas, C. Moreno-Castilla, F. Carrasco-Marín, and A. F. Pérez-Cadenas, "Surface Chemistry, Porous Texture, and Morphology of N-Doped Carbon Xerogels" *Langmuir* **2009**, *25*, 466−470.

[44] J. Yu, M. Guo, F. Muhammad, A. Wang, F. Zhang, Q. Li, and G. Zhu, "One-pot synthesis of highly ordered nitrogen-containing mesoporous carbon with resorcinol–urea–formaldehyde resin for CO_2 capture" *Carbon* **2014**, *69*, 502−514.

[45] X. Ning, H. Ishida, "Phenolic materials via ring-opening polymerization: Synthesis and characterization of bisphenol-A based benzoxazines and their polymers" *J. Polym. Sci., Part A: Polym. Chem.* **1994**, *32*, 1121−1129.

[46] S. Mahadik-Khanolkar, S. Donthula, C. Sotiriou-Leventis, and N. Leventis "Polybenzoxazine Aerogels. 1. High-Yield Room-Temperature Acid-Catalyzed Synthesis of Robust Monoliths, Oxidative Aromatization, and Conversion to Microporous Carbons" *Chem. Mater.* **2014**, *26*, 1303-1317.

[47] D.-C. Guo, J. Mi, G.-P. Hao, W. Dong, G. Xiong, W.-C. Li, H.-J. Bongard, and A.-H. Lu, "Ionic liquid C16mimBF4 assisted synthesis of poly(benzoxazine-co-resol)-based hierarchically porous carbons with superior performance in supercapacitors" *Energy Environ. Sci.* **2013**, *6*, 652–659.

[48] G.-P. Hao, W.-C. Li, D. Qian, G.-H. Wang, W.-P. Zhang, T. Zhang, A.-Q. Wang, F. Schüth, H.-J. Bongard, and A.-H. Lu, "Structurally Designed Synthesis of Mechanically Stable Poly(benzoxazine-co-resol)-Based Porous Carbon Monoliths and Their Application as High-Performance CO_2 Capture Sorbents" *J. Am. Chem. Soc.* **2011**, *133*, 11378–11388

[49] For a recent review, see: S. Chabi, C. Peng, D. Hu, and Y. Zhu, "Ideal three-dimensional electrode structures for electrochemical energy storage" *Adv. Mater.* **2014**, *26*, 2440–2445

[50] For a recent review, see: D. Carriazo, M. C. Serrano, M. C. Gutiérrez, M. L. Ferrer, and F. del Monte, "Deep-eutectic solvents playing multiple roles in the synthesis of polymers and related materials" *Chem. Soc. Rev.* **2012**, *41*, 4996–5014.

[51] A. P. Abbott, G. Capper, D. L. Davies, R. K. Rasheed, and V. Tambyrajah, "Novel solvent properties of choline chloride/urea mixtures" *Chem. Commun.* **2003**, 70–71.

[52] A. P. Abbott, R. C. Harris, and K. S. Ryder, "Application of Hole Theory to Define Ionic Liquids by their Transport Properties" *J. Phys. Chem. B* **2007**, *111,* 4910–4913

[53] A. P. Abbott, G. Capper, and S. Gray, "Design of Improved Deep Eutectic Solvents Using Hole Theory" *ChemPhysChem.* **2006**, *7,* 803–806.

[54] A. P. Abbott, D. Boothby, G. Capper, D. L. Davies, and R. K. Rasheed, "Deep Eutectic Solvents Formed between Choline Chloride and Carboxylic Acids: Versatile Alternatives to Ionic Liquids" *J. Am. Chem. Soc.* **2004**, *126,* 9142–9147.

[55] For a recent review, see: F. del Monte, D. Carriazo, M. C. Serrano, M. C. Gutiérrez, and M. L. Ferrer, "Deep Eutectic Solvents in Polymerizations: A Greener Alternative to Conventional Syntheses" *ChemSusChem* **2014**, *7*, 999 – 1009

[56] D. Carriazo, M. C. Gutiérrez, M. L. Ferrer, and F. del Monte, "Resorcinol-Based Deep Eutectic Solvents as Both Carbonaceous Precursors and Templating Agents in the Synthesis of Hierarchical Porous Carbon Monoliths" *Chem. Mater.* **2010**, *22*, 6146–6152.

[57] D. Carriazo, M. C. Gutiérrez, R. Jiménez, M. L. Ferrer, and F. del Monte, "Deep-Eutectic-Assisted Synthesis of Bimodal Porous Carbon Monoliths with High Electrical Conductivities" *Part. Part. Sys. Charact.* **2013**, *30*, 316–320.

[58] D. Carriazo, M. C. Gutiérrez, F. Picó, J. M. Rojo, J. L. G. Fierro, M. L. Ferrer, and F. del Monte, "Phosphate-Functionalized Carbon Monoliths from Deep Eutectic Solvents and their Use as Monolithic Electrodes in Supercapacitors" *ChemSusChem.* **2012**, *5*, 1405–1409.

[59] M. C. Gutiérrez, D. Carriazo, C. O. Ania, J. L. Parra, M. L. Ferrer, and F. del Monte, "Deep Eutectic Solvents as Both Precursors and Structure Directing Agents in the Synthesis of Nitrogen Doped Hierarchical Carbons Highly Suitable for CO_2 Capture" *Energy Environ. Sci.* **2011**, *4*, 4201–4210.

[60] J. Patiño, M. C. Gutiérrez, D. Carriazo, C. O. Ania, J. L. G. Fierro, M. L. Ferrer and F. del Monte, "DES Assisted Synthesis of Hierarchical Nitrogen-Doped Carbon Molecular Sieves for Selective CO2 versus N2 Adsorption" *J. Mater. Chem. A* **2014**, *2*, 8719-8729

[61] N. López-Salas, E. Oliveira-Jardim, A. Silvestre-Albero, M. C. Gutiérrez, M. L. Ferrer, F. Rodriguez-Reinoso, J. Silvestre-Albero, and F. del Monte, "Use of Eutectic Mixtures for Preparation of Monolithic Carbons with CO_2-Adsorption and Gas-Separation Capabilities"" *Langmuir* **2014** Submitted

[62] K. Siimer, T. Kaljuvee, P. Christjanson, T. Pehk, and I. Saks, "Effect of alkylresorcinols on curing behavior of phenol-formaldehyde resol resin" *J. Therm. Anal. Calorim.* **2008**, *91*, 365–373

[63] P. P. Kalbende, Ma. V. Tarase, A. B. Zade, "Preparation, Characterization, and Thermal Degradation Studies of p-Nitrophenol-Based Copolymer" *J. Chem.* **2013**, Article ID 846327

[64] J. Patiño, M. C. Gutiérrez, D. Carriazo, C. O. Ania, J. L. Parra, M. L. Ferrer and F. del Monte, "Deep eutectic assisted synthesis of carbon adsorbents highly suitable for low-pressure separation of CO_2–CH_4 gas mixtures" *Energy Environ. Sci.* **2012**, *5*, 8699–8707.

[65] W. Xu, E. I. Cooper, and C. A. Angell, "Ionic Liquids: Ion Mobilities, Glass Temperatures, and Fragilities" *J. Phys. Chem. B* **2003**, *107*, 6170–6178

[66] M. C. Gutiérrez, M. L. Ferrer, C. R. Mateo, and F. del Monte, "Freeze-Drying of Aqueous Solutions of Deep Eutectic Solvents: A Suitable Approach to Deep Eutectic Suspensions of Self-Assembled Structures" *Langmuir* **2009**, *25*, 5509–5515

[67] M. C. Gutiérrez, F. Rubio, and F. del Monte, "Resorcinol-Formaldehyde Polycondensation in Deep Eutectic Solvents for the Preparation of Carbons and Carbon-Carbon Nanotube Composites" *Chem. Mater.* **2010**, *22*, 2711–2719

[68] M. C. Gutiérrez, M. L. Ferrer, L. Yuste, F. Rojo, and F. del Monte, "Bacteria Incorporation in Deep-eutectic Solvents through Freeze-Drying" *Angew. Chem.* **2010**, *49*, 2158–2162.

[69] Y. Chen, Z. Chen, S. Xiao, and H. Liu, "A novel thermal degradation mechanism of phenol–formaldehyde type resins" *Thermochim. Acta*, 2008, **476**, 39–43.

[70] N. Liu, L. Yin, C. Wang, L. Zhang, N. Lun, D. Xiang, Y. Qi, and R. Gao, "Adjusting the texture and nitrogen content of ordered mesoporous nitrogen-doped carbon materials prepared using SBA-15 silica as a template" *Carbon* **2010**, *48*, 3579–3591.

[71] Y. Qiu and L. Gao, "Chemical synthesis of turbostratic carbon nitride, containing C–N crystallites, at atmospheric pressure" *Chem. Commun.* **2003**, 2378–2379.

[72] D. C. Nesting and J. V. Badding, "High-Pressure Synthesis of sp^2-Bonded Carbon Nitrides" *Chem. Mater.* **1996**, *8*, 1535–1539.

[73] I. L. Moudrakovski, C. I. Ratcliffe, J. A. Ripmeester, L. Q. Wang, G. J. Exarhos, T. F. Baumann and J. H. Satcher, "Nuclear Magnetic Resonance Studies of Resorcinol–Formaldehyde Aerogels" *J. Phys. Chem. B* **2005**, *109*, 11215–11222.

[74] S. Mulik, C. Sotiriou-Leventis and N. Leventis, "Time-Efficient Acid-Catalyzed Synthesis of Resorcinol-Formaldehyde Aerogels" *Chem. Mater.* **2007**, *19*, 6138–6144.

[75] E. Pretsch, P. Buhlmann, and C. Affolter, "Structure Determination of Organic Compounds: Tables of Spectral Data" Springer, 2000, Germany, 404.

[76] K. Nakanishi and N. Soga, "Phase Separation in Silica Sol-Gel System Containing Poly(Ethylene oxide) II. Effects of Molecular Weight and Temperature" *Bull. Chem. Soc. Jpn.*, **1997**, *70*, 587–592.

[77] H. Kaji, K. Nakanishi, N. Soga, T. Inoue, and N. Nemoto "In situ Observation of Phase Separation Processes in Gelling Alkoxy-Derived Silica System by Light Scattering Method" *J. Sol-Gel Sci Technol.* **1994**, *3*, 169–188.

[78] F. Kapteijn, J. A. Moulijn, S. Matzner and H.-P. Boechm, "The development of nitrogen functionality in model chars during gasification in CO_2 and O_2" *Carbon*, **1999**, *37*, 1143–1150.

[79] J. R. Pels, F. Kapteijn, J. A. Moulijn, Q. Zhu and K. M. Thomas, "Evolution of nitrogen functionalities in carbonaceous materials during pyrolysis" *Carbon*, **1995**, *33*, 1641–1653.

Table 1 – Chemical shifts obtained by ^{1}H NMR spectroscopy **–** at room temperature and using $CDCl_3$ as reference solvent **–**of resorcinol (Re), 4-Hexylresorcinol (4Re), *p*-nitrophenol (pNP) and choline chloride (ChCl), and the eutectic mixtures prepared with different molar ratios of the components ($N1_{DES}$, $N2_{DES}$ and $N3_{DES}$). Deuterated $CDCl_3$ was used as the external reference.

Sample	δ (ppm)														
	Re			4Re							pNP		ChCl		
	H at C5	**H** at C4&6	**H** at C2	**H** at C12	**H** at C11-9	**H** at C8	**H** at C7	**H** at C6	**H** at C5	**H** at C2	**H** at C3&5	**H** at C2&5	**H** at C2	**H** at C1	**H** at NCH_3
Re	7.0 (1H)	7.4 (2H)	6.3 (1H)												
4Re				0.9 (3H)	1.3 (6H)	1.5 (2H)	2.5 (2H)	6.3 (1H)	6.9 (1H)	6.3 (1H)					
pNP											8.1 (2H)	6.9 (2H)			
ChCl													4.1 (2H)	3.6 (2H)	3.2 (9H)
$N1_{DES}$	6.1 (1H)	5.9 (2H)	*5.8 (1H)	0.0 (3H)	0.4 (6H)	0.7 (2H)	1.7 (2H)	*5.8 (1H)	6.0 (1H)	*5.8 (1H)	7.2 (2H)	6.1 (2H)	3.2 (2H)	2.5 (2H)	2.2 (9H)
$N2_{DES}$	**6.2 (1H)	**6.2 (2H)	*5.8 (1H)	0.0 (3H)	0.3 (6H)	0.7 (2H)	1.7 (2H)	*5.8 (1H)	6.0 (1H)	*5.8 (1H)	7.1 (4H)	**6.2 (4H)	3.3 (2H)	2.6 (2H)	2.3 (9H)
$N3_{DES}$	6.3 (1H)	6.0 (2H)	*5.8 (1H)	0.0 (3H)	0.4 (6H)	0.7 (2H)	1.7 (2H)	*5.8 (1H)	6.2 (1H)	*5.8 (1H)	7.1 (6H)	6.2 (6H)	3.4 (2H)	2.7 (2H)	2.4 (9H)

* These peaks are all included in the signal at 5.8 ppm.
** These peaks are all included in the signal at 6.2 ppm.

Table 2 – Nitrogen doping efficiency and carbon conversion reached after condensation and carbonization – temperatures and times are also included – of different nitrogen-rich carbon precursors. The table also includes information with regard to the use of structure directing agents to obtain hierarchical porous structures.

Ref.	Carbon precursors	Molar ratio	T (°C) / t (h)	Initial N/C wt%	Final N/C wt%	Nitrogen doping efficiency %	Carbon conversion wt%	HPM or HPP / SDA[a]
	Resorcinol 4-Hexylresorcinol ***p-Nitrophenol*** Choline Chloride	1:1:**1**:1	400/4 500/4 600/4 800/4	4.6	3.0 3.2 3.3 3.6	65.7 71.4 70.9 78.3	64 62 57 50	HPM/No
		1:1:**2**:1	400/4 500/4 600/4 800/4	7.2	3.9 4.2 4.0 3.9	55.0 58.3 55.1 54.2	62 61 58 52	HPM/No
		1:1:**3**:1	400/4 500/4 600/4 800/4	8.9	4.7 4.9 4.4 3.8	52.7 58.3 49.8 42.7	63 60 56 50	HPM/No
2	**Melamine**	**1**	650/1 750/1 800/1 850/1 1000/1	70	48.8 46.8 44.7 35.4 14.8	69.8 66.9 63.9 50.6 21.3	42 39 36 35 30	HPP/Yes
37	Phenol ***Melamine***	1:**0.5**	800/3	31.8	4.7	14.7	-	P[a]/Yes
		1:**1**	800/3	43.8	8.9	20.3	-	
		1:**2**	800/3	53.8	13.3	24.7	-	
38	Phenol ***Melamine***	1:**0.8**	800/3	40.0	3.7	9.2	-	M[a]/Yes
39	Resorcinol ***3-hydroxypyridine***	1:**1**	500/1	9.6	0.9[b]	-	38	HPP/No
	Resorcinol ***3-aminophenol***	9:**1**	500/1	1.9	5.0[b]	-	53	HPP/No
	Resorcinol ***Melamine***	4:**1**	500/1	20.6	7.9[b]	-	40	HPP/No
40	Resorcinol ***Melamine***	5:**1**	800/2	17.5	3.5[c]	-	-	HPP/No
	Resorcinol ***Urea***	2:**1**	800/2	25.0	2.7[c]	-	-	HPP/No
41	Resorcinol ***Melamine***	1:**0.2**	600/3 700/3 800/3	17.5	3.17 2.72 2.49	18.1 15.5 14.2	-	HPP/Yes
42	m-cresol ***Methylated melamine***	2.2: **1**	800/2	18.7	2.8	-	-	HPM/No
43	***melamine*** ***3-hydroxyaniline***	**1:0.6**	500/5 700/5 900/5	53.8	14.6 9.9 6.5	27.1 18.4 12.1	48 45 50	HPP/No
	Resorcinol	1:**0.6**	500/5	9.6	10.8	>100	49	HPP/No

	3-hydroxypyridine		700/5 900/5		5.5 4.4	57.3 47.3	41 38	
	Resorcinol ***Melamine***	1:**0.6**	500/5 700/5 900/5	35.0	5.7 4.2 4.2	16.3 12.0 12.0	62 54 51	HPP/No
44	Resorcinol ***Urea***	1:**1**	550/3 700/3 800/3	25.0	4.31 2.82 2.64	17.2 11.3 10.6	-	HPP/Yes
45	Resorcinol ***Lysine***	7.8:**1**	400/-- 500/-- 600/-- 700/-- 800/--	4.2	2.36 2.17 2.06 1.49 1.33	56.2 51.7 49.0 35.5 31.7	-	HPM/No
47	Bisphenol-A ***Aniline***[c]	1:**2**	200/5 300/5 400/5 500/5 600/5 800/5	7.9	5.6 6.0 6.5 6.0 5.6 4.6	70.9 75.9 82.3 75.9 70.9 58.0	56 - 61	HPM/No
	Bisphenol-A ***Aniline***[d]	1:**2**	200/5 300/5 400/5 500/5 600/5 800/5	7.9	5.4 5.2 5.2 5.4 5.5 4.3	68.3 65.8 65.8 68.3 69.6 54.4	56 - 61	HPM/No
48	Resorcinol C16mimBF4 ***1,6-diaminohexane***	20:2:**1**	800/--	1.9	0.8	42.1	-	HPM/Yes
49	Resorcinol ***1,6-diaminohexane***	6.8:**1**	800/2	4.8			-	HPM/Yes
59	Resorcinol ***3-hydroxypyridine***	1:**1**:1[e]	600/4 800/4	9.6	6.59 4.82	68.6 50.2	80 70	HPM/No
		2:**2**:1[e]	600/4 800/4	9.6	7.08 5.27	73.7 54.9	80 70	HPM/No
60	Resorcinol ***3-hydroxypyridine***	1:**2**	450/4 500/4 600/4 700/4 800/4	12.7	7.6[f] 7.7[f] 7.7[f] 6.6[f] 3.7[f]	-	81 74 67 66 54	HPM/No
		1:**3**	450/4 500/4 600/4 700/4 800/4	14.3	8.7[f] 8.7[f] 8.1[f] 7.4[f] 5.4[f]	-	81 76 72 68 52	HPM/No

[a] HPM stands for "hierarchical porous monolith", HPP stands for "hierarchical porous powder", SDA stands for "structure directing agent", P stands for "powder" and M stands for "monolith".

[b] Theoretical maximum.

[d] Hydrothermal synthesis.

[c] Catalyzed synthesis.

[e] DES-assisted co-condensation with Choline Chloride as the hydrogen bond acceptor of the DES.

[f] Data obtained from XPS.

Table 3 – Data obtained from N_2 (at –196 °C, grey columns) and CO_2 (at 0 °C, white columns) adsorption-desorption isotherms for $N1_{C@800}$, $N2_{C@800}$ and $N3_{C@800}$.

Sample	S_{BET} (m^2/g)	$V_{total\ pores}$ (cm^3/g)[a]	W_o (cm^3/g)	L (nm)	E_0 (kJ/mol)	CO_2-uptake at 0 – 25 °C (mmol/g)
$N1_{C@800}$	15	0.014	0.309	0.56	30.8	3.8 – 2.8
$N2_{C@800}$	16	0.014	0.288	0.55	31.2	3.7 – 2.7
$N3_{C@800}$	13	0.022	0.353	0.56	30.8	4.2 – 3.3

[a] Calculated at $P/P_0 = 0.99$

Table 4 – CO_2-uptake at 25 °C found for $N1_{C@800}$, $N2_{C@800}$ and $N3_{C@800}$, and for some of the most remarkable NPCs found in the literature. Nitrogen content is also included for comparison.

Sample	Reference	Nitrogen content (wt%)	CO_2-uptake at 25 °C (mmol/g)
$N1_{C@800}$	This work	3.6	2.8
$N2_{C@800}$	This work	3.9	2.7
$N3_{C@800}$	This work	3.8	3.3
$C_{RHC221\text{-}DES@800}$	60	4.2	3.3
$C_{RHC111\text{-}DES@800}$	60	4.7	3.0
$C_{ReHy12@800}$	61	3.7	2.7
$C_{ReHy13@800}$	61	5.4	2.7
IBN9-NC-600	9	18.8	2.2
IBN9-NC-600K[a]	9	12.8	3.7
SBA-NC-900	10	17.4	2.3
SBA-NC-900K[a]	10	10.5	4.0
H-NMC-2.5	11	13.1	0.3
H-NMC-2.5-K[a]	11	6.7	3.2
AC2-700	12	1.9	3.5
AC2-800	12	1.3	3.1
CP2-600	13	10.1	3.9
CP2-800	13	0.8	2.7
CN-850	13	2.9	3.1
CN-950	13	4.3	4.3
RFL-700	14	1.4	3.1
RFL-800	14	1.3	2.8
SK-0.5-700[a]	17	0.28[b]	4.2
SK-0.5-800[a]	17	0.15[b]	4.0

[a] Carbons submitted to KOH activation. [b] Nitrogen content from XPS

Figure 1 - DSC traces taken at a rate of 5 °C/min of $N1_{DES}$, $N2_{DES}$ and $N3_{DES}$. Samples neither display a melting point (T_m) nor crystallization temperature (T_c). Samples only displayed a glass-transition temperature (T_g) in between – 49 °C and – 57 °C.

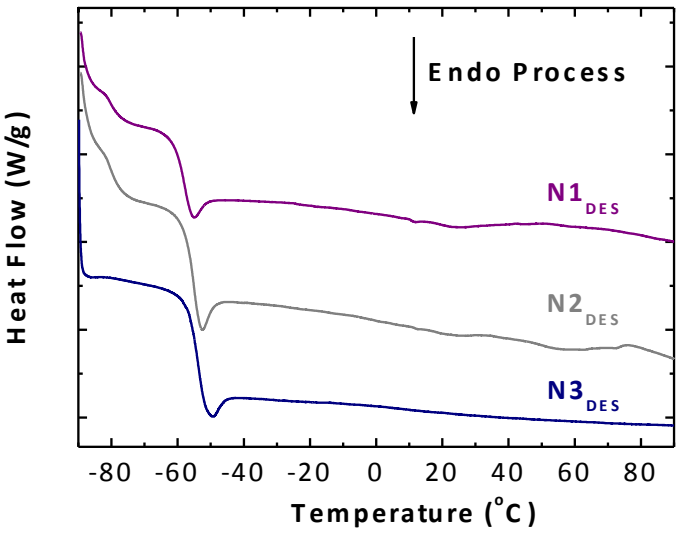

Figure 2 – ^{1}H NMR spectra (at room temperature and using $CDCl_3$ as the external reference) of $N1_{DES}$, $N2_{DES}$ and $N3_{DES}$.

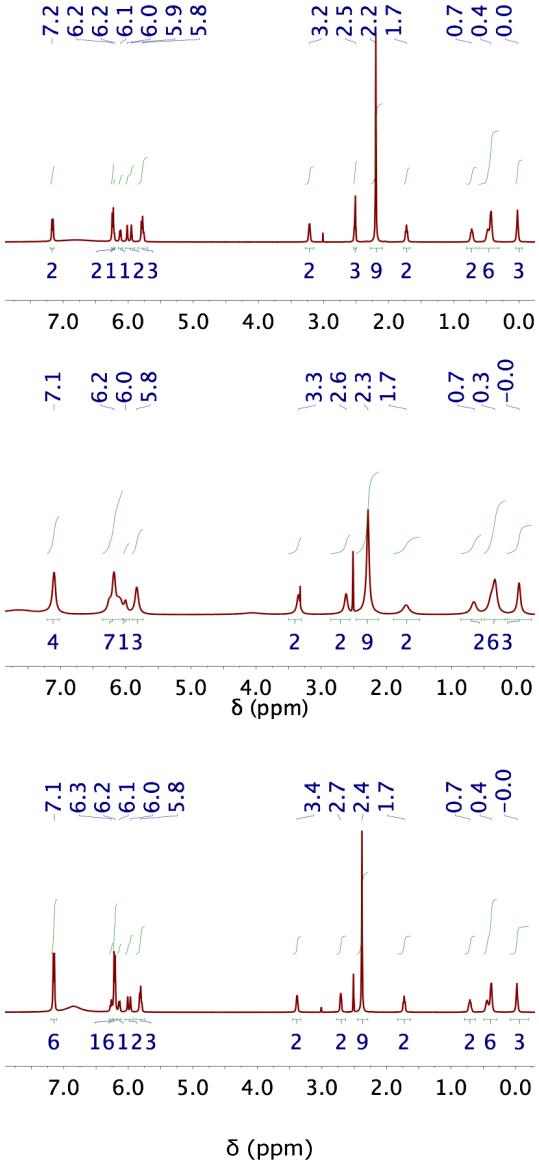

Figure 3 – Monoliths obtained right after polycondensation ($N1_{GEL}$, $N2_{GEL}$ and $N3_{GEL}$ in top panel) and after carbonization at 800 °C ($N1_{C@800}$, $N2_{C@800}$ and $N3_{C@800}$ in bottom panel). Interestingly, the resulting carbons were susceptible of polishing so the final in-height-dimensions of the monoliths can be adjusted without compromising the monolithic form.

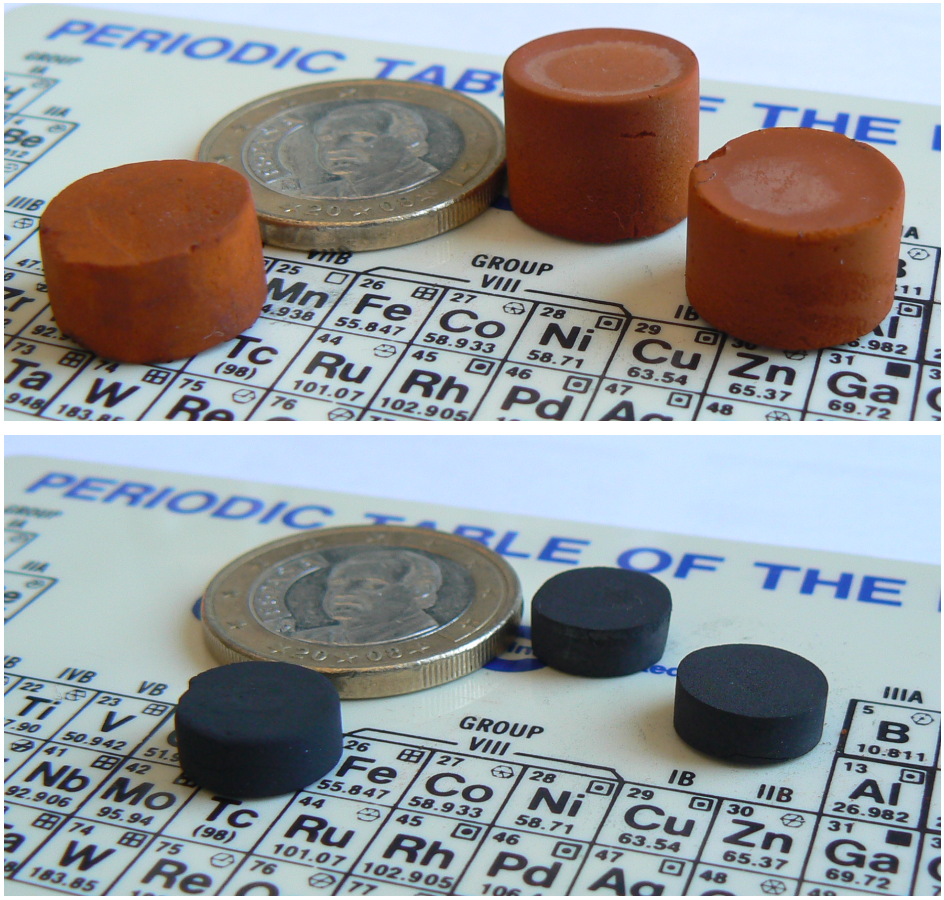

Figure 4 – Fourier transform infrared (FTIR) spectra of (from top to bottom) $N1_{GEL}$, $N2_{GEL}$ and $N3_{GEL}$.

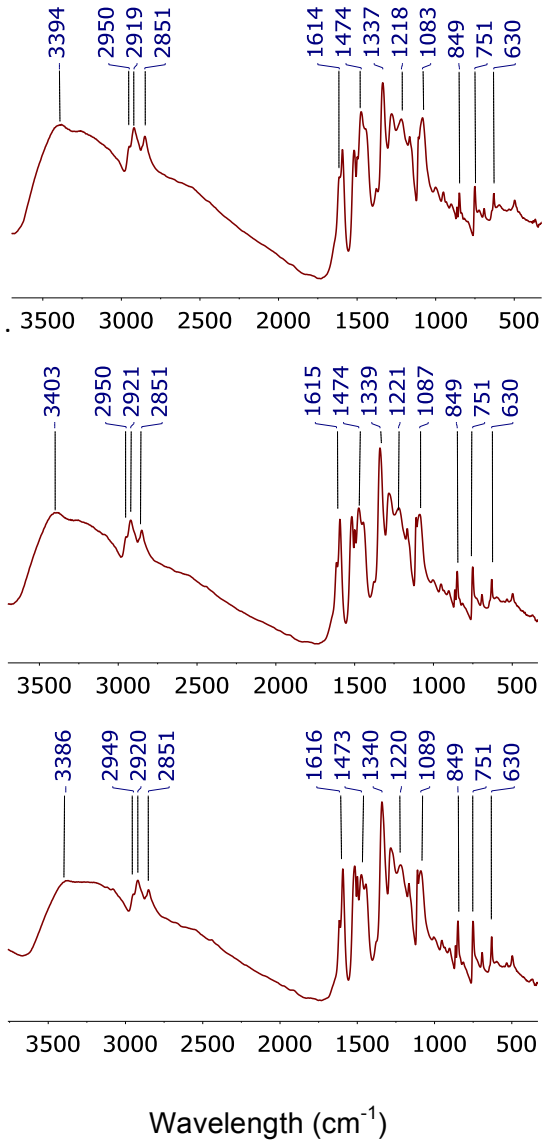

Figure 5 – Solid-state ^{13}C CPMAS NMR spectra of (from top to bottom) $N1_{GEL}$, $N2_{GEL}$ and $N3_{GEL}$.

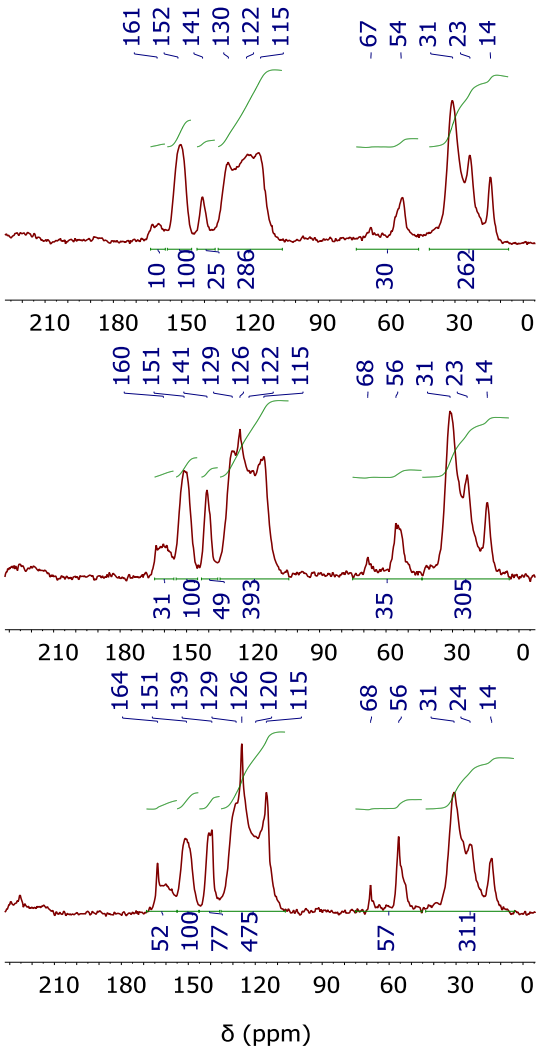

Figure 6 – SEM micrographs of (from top to bottom) $N1_{GEL}$, $N2_{GEL}$ and $N3_{GEL}$.

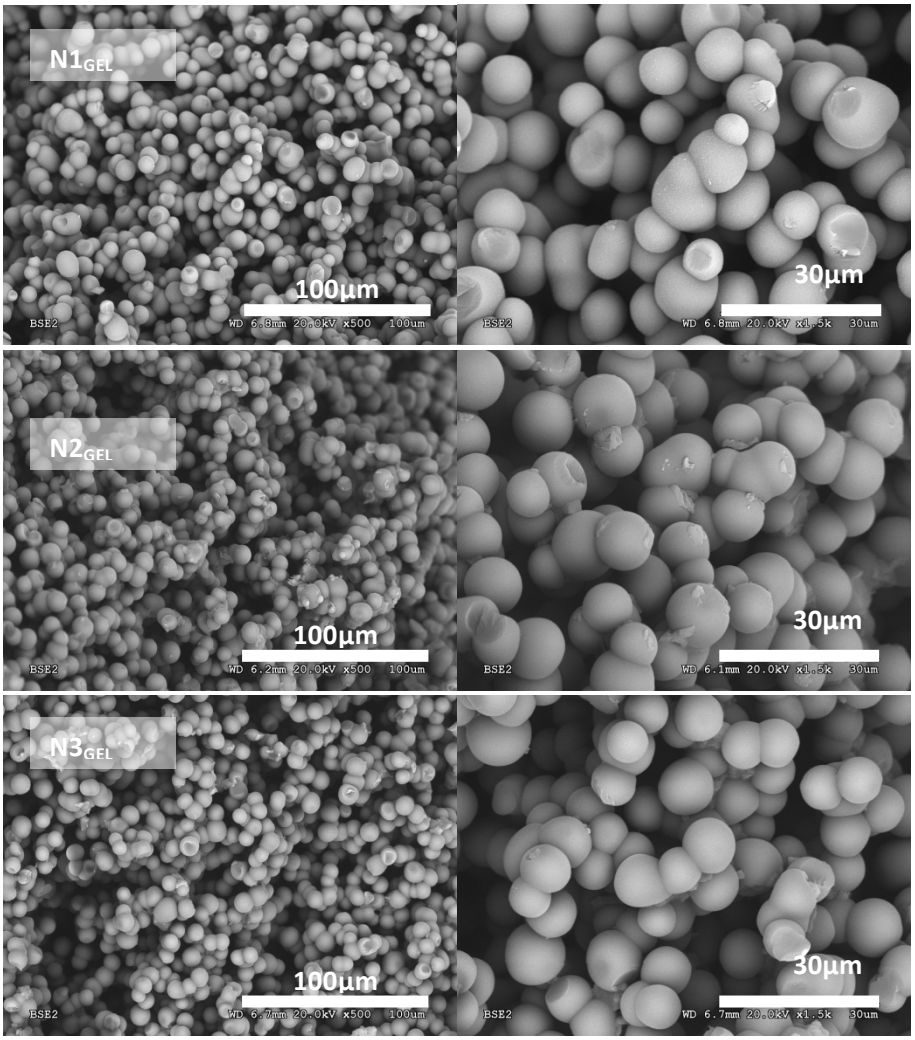

Figure 7 – SEM micrographs of (from top to bottom) $N1_{C@800}$, $N2_{C@800}$ and $N3_{C@800}$.

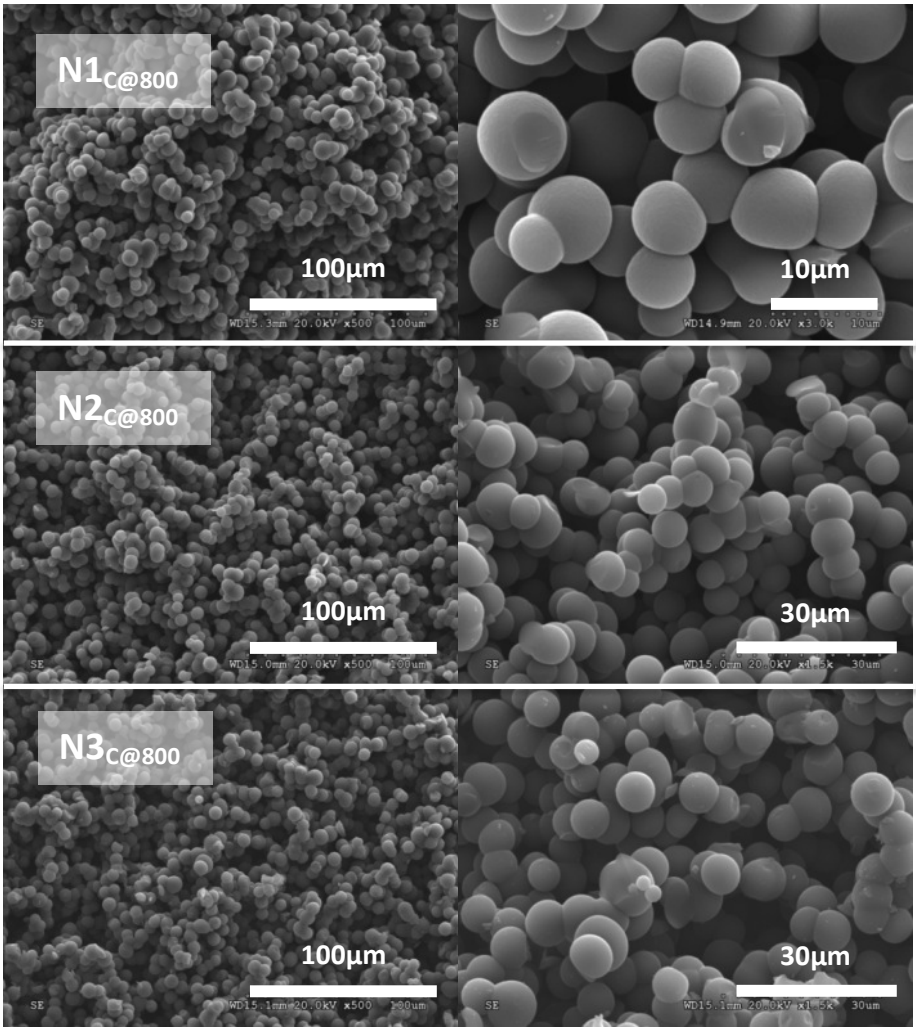

Figure 8 – Plot representing the nitrogen content of $N1_{C@x}$, $N2_{C@x}$ and $N3_{C@x}$ – x= 400, 500, 600 and 800 °C – versus the pNP molar ratio at $N1_{DES}$, $N2_{DES}$ and $N3_{DES}$.

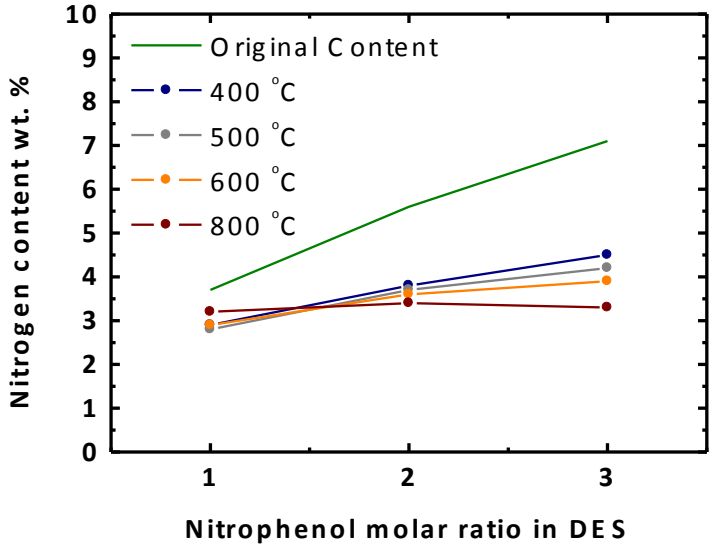

Figure 9 – XPS N1s spectra of (from top to bottom) $N3_{C@500}$ and $N3_{C@800}$. The solid black line represents the as-acquired-spectrum, the solid lines with circles in blue represent the components resulting from deconvolution, and the solid circles in black are the fitting curves resulting from the addition of each contribution.

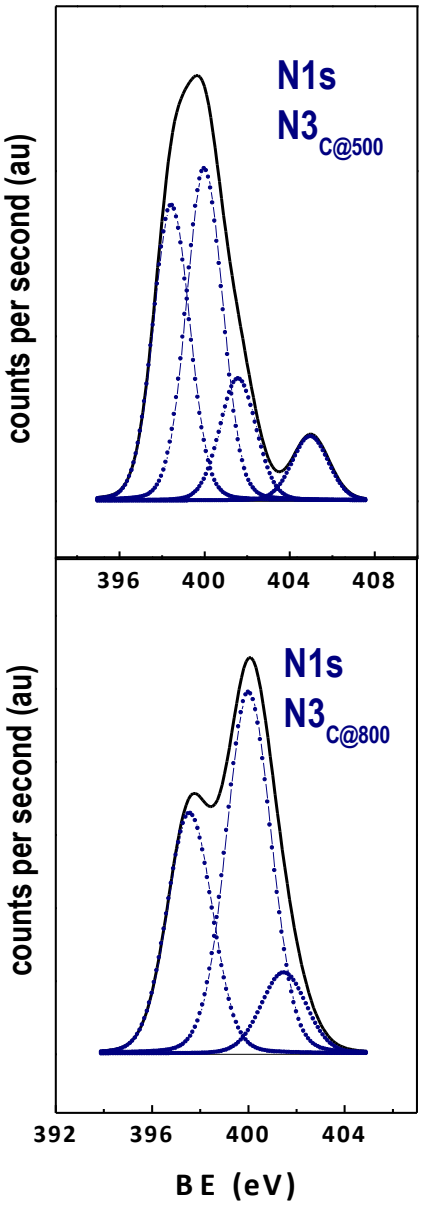

Figure 10 – CO_2 adsorption desorption isotherms measured at 0 °C and 25 °C for $N1_{C@800}$, $N2_{C@800}$ and $N3_{C@800}$.